REPORT NO. 95

DECEMBER, 1955

THE COLLEGE OF AERONAUTICS

CRANFIELD

The Flexure-Torsion Flutter of Cambered Aerofoils in Cascade

by

Arthur H. Craven, D.Sc., Ph.D., D.C.Ae.,

and

Ian Davidson, B.Sc., D.C.Ae.

SUMMARY

This report contains the results of a series of tests on the flexure-torsion flutter of cascades of aerofoils of 30° and 45° camber. The critical flutter speeds and frequencies in cascade are expressed as ratios of the values for the aerofoil in the isolated condition. The tests cover stagger angles between -30° and $+30^{\circ}$ and gap chord ratios up to 1.5 at a Reynolds number of 1×10^5 based on aerofoil chord.

It was found that the effect of camber was to increase the critical flutter speed ratio and to decrease the critical frequency ratio. The flutter characteristics also depended on the magnitude and sign of the stagger angle. Limited tip clearance was shown to reduce the flutter speed ratio but to have little effect on the critical flutter frequency ratio. Small angles of incidence were found to have negligible effect on the characteristics. It was noted that adjacent aerofoils were oscillating approximately 180° out of phase.

CONTENTS

LIST OF SYMBOLS

c	aerofoil chord
$F(l)$	static mode in torsion
$f(l)$	static mode in flexure
f_{crit}	critical flutter frequency of isolated aerofoil
f'_{crit}	critical flutter frequency of cascade
k	reduced frequency of the isolated aerofoil $\left(\frac{\omega c}{2q_1}\right)$
k'	reduced frequency of the cascade
l	ratio of spanwise distance to complete span
q_1	free stream fluid speed
s	gap, measured along the line of 1/4 c points, i.e. along y' axis
V_{crit}	critical flutter speed of isolated aerofoil
V'_{crit}	critical flutter speed of cascade
$\left(V_{crit}\right)_{a_1=o}$	critical flutter speed of isolated aerofoil at zero incidence
x,y	rectangular coordinates (the x-axis coincides with the chord line of the aerofoil in the static case)
y'	coordinate axis through O inclined at angle β to the y axis
a	incidence relative to the x axis
a_1	inflow angle
β	stagger angle
γ	camber angle
ω	circular frequency of the oscillation

A prime denotes a value for the cascade and a suffix 'crit' denotes a critical value of the variable.

1. Introduction

The behaviour of aerofoils fluttering in cascade and in particular the effect of the adjacent blades in the cascade on the flutter characteristics of the isolated aerofoil have been the subject of papers by Bellenot and Lalive d'Epinay (1) and Lilley (2). The first paper describes some flutter tests on cambered aerofoils in cascade at one gap-chord ratio over a range of angles of stagger. The report by Lilley gives the results of an experimental investigation into the flexure-torsion flutter of symmetrical aerofoils in cascade over a range of gap-chord ratios and stagger angles. That report also contains a theory setting up the two-dimensional lift and moment equations for an unstaggered cascade of thin symmetrical aerofoils and expressions for the flutter derivatives are deduced. This theory depends upon the experimental observation that the aerofoils oscillate in anti-phase and in consequence the problem reduces to that of a single aerofoil oscillating between parallel flat plates. The present writers also had access to the results of some experimental work on cascades of symmetrical blades by Sheikh (3) where the emphasis was on repeatability of results and which confirmed the work reported by Lilley.

The lift and moment equations for thin aerofoils oscillating in an infinite unstaggered cascade have also been developed by Mendelson and Carroll (4). In this development the usual assumptions of thin aerofoil theory are used and thus the results are applicable only to a cascade of aerofoils of small camber. Sisto (5) has presented a theory in which a general expression for the vorticity at any point on the oscillating aerofoil is given in the form of an integral equation involving the induced velocity, the angle of stagger and the phase difference between adjacent blades. This equation is solved approximately for the case of zero stagger only and numerical results for the lift and moment derivatives are given for various values of phase angle, reduced frequency and gap/chord ratio. These results agree with the exact calculations of Mendelson and Carroll and the approximate calculations of Lilley.

Legendre (6) has considered the general case of the flutter of a cascade with stagger. This is an extension of the work of Timman for the case of zero stagger. Expressions are given for the velocity potential and circulation from which the pressure distribution can be determined. Eichelbrenner (7) gives details of calculations based on Legendre's method for one gap/chord ratio and stagger angle. He simplifies Legendre's expressions by extended use of theta and zeta functions and produces curves for the work due to damping to be zero for various values of reduced frequency. These curves are compared with corresponding

ones for the isolated aerofoil. It should be noted that the use of Legendre's criterion for flutter, i.e. that the work due to the aerodynamic damping during one cycle is zero, entails a simpler calculation than that of the individual aerodynamic derivatives. The calculation of the latter are essential before a comparison can be made between theoretical critical flutter speeds and those obtained by the experiment reported in this paper.

The purpose of this paper is to present the results of an investigation into the flexure-torsion flutter of cambered aerofoils in cascade performed between January and May 1955. In order that the models would flutter within the speed range of the tunnel and to provide a basis for ready comparison with the results for symmetrical blades given in (2), the aerofoils were again made with a light silk covered wooden framework. The results are presented in a similar form.

2. Apparatus

2.1. The wind tunnel

The experiments were conducted in a blower type wind tunnel in the Aerodynamics laboratory of the College of Aeronautics. The tunnel working section dimensions were 18.75in. x 8.75in. The speed range was from zero to 170 feet per second, the velocity distribution across the working section in the plane of the aerofoils being uniform to within $\pm$ .5 per cent. (See figs. 6 and 7). The Reynolds number based on blade chord was approximately 10^5. The wind speed in the centre of the working section was calibrated at the centre model attachment position against the difference between the static pressure at a tapping in the settling chamber and atmospheric pressure (see fig. 8).

A turntable was mounted in a side-wall extension of the tunnel contraction. A series of holes at 3/4in. centres was drilled along a diameter of the turntable and through these holes the extensions of the aerofoil spars were placed, and locked by clamping bars on the reverse side. A general view of the tunnel, measuring equipment and the models in position is given in fig. 1.

A smoke generator was used to give a single filament of smoke over the centre of reference blade of the cascade.

For pilot experiments on the effect of tip clearance, a perspex plate 3ft x 2ft x $\frac{1}{2}$in. with a faired nose was placed near the tip so that the clearance between

the tips of the blades and the plate was variable. A photograph of the plate in position is shown in fig. 2.

2.2. The models

The aerofoils were of rectangular planform of 3in. chord and 8in. span and had a mahogany spar 1/8in x 3/16in at the quarter chord point, and eight mahogany ribs 1/8in thick, evenly spaced along the spar. The covering was silk treated with a mixture of thinners and vaseline.

Two sets of aerofoils were made; the first having a N.A.C.A. 0010 section on a 30° camber line and the second having a N.A.C.A. 0010 section on a 45° camber line. A part sectional view and a detailed drawing of a model are given in figs. 3 and 4.

The flexural and torsional stiffnesses, and the static modes of the aerofoils were measured by static load tests, and the natural frequencies in flexure and torsion were measured on a vibrating table (see reference 2).

2.3. Instruments

During the tests the wind speed was obtained from readings of static pressure in the settling chamber measured on a Betz manometer. The flutter frequency was measured by a strobo-tachometer and by an E.M.I. type 3B stroboflash capable of readings up to 6000 cycles per minute.

To assist in the study of the blade motion and flow visualisation, film records were taken using.-

i) a Paillard-Bolex cine camera running at 64 frames per second with 1in. and 2in. lenses at f.16. Illumination was provided by a 2kw spot and two 500 watt flood lights.

ii) an Eastman high speed camera type 3, fitted with a rotating block shutter and running up to 3000 frames per second. A 2in lens was used at f.2.7. For this camera the previous lighting was augmented by a 1kw. spot light. *

The film used in both cases was Kodak Super XX. Figure 5 shows the arrangement used with the Paillard-Bolex camera. A similar arrangement was used with the Eastman high speed camera.

---

* This camera was lent and operated by the Instrumentation Department of the Royal Aircraft Establishment, Farnborough.

3. Scope of the Tests

The effects of gap-chord ratio and stagger angle were investigated for both the 30° camber aerofoils and the 45° camber aerofoils. The range of gap-chord ratio was 0.25 to 1.50 and the range of stagger angles +30° to -30°.

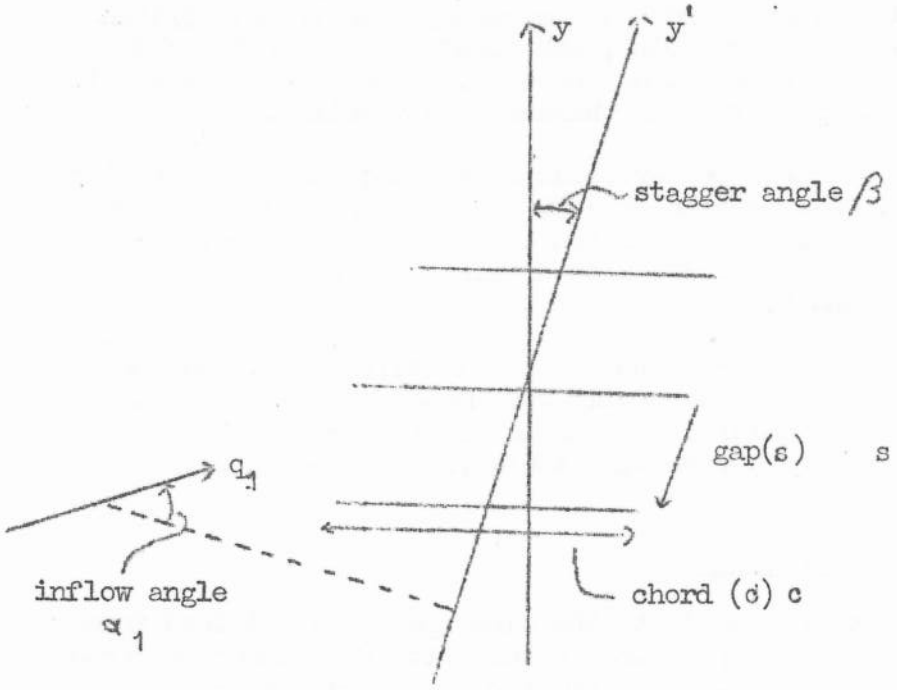

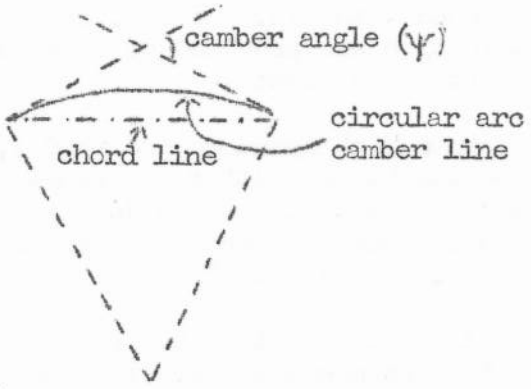

Further tests on the 30° camber aerofoils were

performed to determine the effects of variation of incidence (inflow angle variation $\beta + 2^{\circ}$, $\beta - 2^{\circ}$; β = stagger angle) over the above ranges of gap-chord ratio and stagger angle. Values of incidence greater than these were found to be undesirable because of the violent nature of the flutter.

Preliminary tests on the effect of tip clearance in the range 0.1 to 0.5in. were also made using the 30° camber aerofoils.

Each of the series of tests was repeated on several different occasions to include the effect of ageing and various conditions of temperature and humidity.

4. Test Procedure

Each aerofoil was tested individually and the value of the critical flutter speed and critical frequency were measured. The method used was to increase the wind speed until the aerofoil started fluttering. The wind speed was then reduced and that speed at which the flutter stopped was taken as the critical flutter speed. The critical frequency was obtained by plotting the frequency of one oscillation at a number of steady speeds above the critical and extrapolating to the critical flutter speed. The estimated accuracies of the critical flutter speed and frequency were $\pm$ 0.50 per cent and $\pm$ 1.0 per cent respectively.

The cascade was then chosen such that the isolated characteristics of the members differed by less than $\pm$ 5 per cent. One of the weaker aerofoils was taken as a control and placed in the centre of the cascade and values of critical speed and frequency were determined for this aerofoil by the method described above. These values, however, were not accepted unless each member had the same frequency at speeds above the critical and the cascade stopped fluttering as a whole. In order to reduce the slight effects of ageing, and of variations of temperature and humidity during a run, the control aerofoil was tested in the isolated condition before and after each cascade test. The mean of the two values so obtained was used to determine the critical speed and frequency ratios of the aerofoil in cascade. In each configuration the test was repeated until several consecutive and consistent readings were obtained.

Cine film records were taken of the cascade fluttering under the conditions found to give the largest variation from the normal flutter at zero stagger. Flow patterns were observed using the stroboflash and recorded with the high speed camera.

5. Experimental Results

5.1. Presentation of results

The main requirement in a study of flutter of a given aerofoil structure is a knowledge of the critical flutter speed, flutter frequency and the reduced frequency of the oscillation. In cascade work it is convenient to consider the ratios of these quantities to their values in the isolated condition and this has the advantage of giving the results in a non-dimensional form. The experimental technique described in section 4 ensures that these ratios are, as far as is possible, independent of the variation of temperature and humidity during the test and the age of the blade.

The important parameters in this study are gap chord ratio, stagger angle and inflow angle. Consequently the results presented in figs. 11-18 show the variation of the non-dimensional ratios with these parameters.

During the tests it was noted that the use of stops to restrict the amplitude of the motion caused considerable variation in the results. After a little practice however, it was found that the amplitude of flutter could be maintained at a reasonable level. The use of stops was then discontinued but a preliminary investigation into the effect of tip clearahce was made. The results of these tests are shown in fig. 19.

Variations of the several ratios have been plotted separately against gap chord ratio and stagger angle in turn for one fixed value of the other parameter. The results for the 30° camber and 45° camber aerofoils in similar configurations are plotted on the same axes. This method has been used to give clearer representation, since to include the results for all values of the fixed parameter would result in an unsatisfactory and confused set of curves. It also provides an immediate comparison for the effects of camber; the values shown for the symmetrical (0° camber) blades being taken from ref. 2.

The details of the graphs presented are as follows:-

fig. 11 The flutter characteristics of the isolated (30° camber) aerofoil.

fig. 12 Variation of $\dfrac{\text{Critical flutter speed for cascade with inflow angle } a_1,\ (V'_{crit})_{a_1}}{\text{Critical flutter speed for isolated aerofoil at zero inflow angle } (V_{crit})_{a_1=0}}$ with gap chord ratio (30° camber, 0° stagger).

fig.13A-E Variation of critical flutter speed ratio V'_{crit}/V_{crit} with gap chord ratio (s/c) for various stagger angles (β).

fig.14A-C Variation of critical flutter speed ratio V'_{crit}/V_{crit} with stagger angle (β) for various gap-chord ratios (s/c)

fig.15A-E Variation of critical flutter frequency ratio (f'_{crit}/f_{crit}) with gap chord ratio (s/c) for various stagger angles (β).

fig.16A-C Variation of critical frequency ratio (f'_{crit}/f_{crit}) with stagger angle (β) for various gap chord ratios (s/c).

fig.17A-D Variation of the reduced frequency ratio (k'/k) with gap-chord ratio (s/c) for various stagger angles (β).

fig.18A-C Variation of the reduced frequency ratio (k'/k) with stagger angle for various values of gap chord ratio (s/c).

fig. 19 Variation of the critical flutter speed ratio $\frac{(V'_{crit})_{finite\ gap}}{(V'_{crit})_{infinite\ gap}}$ with tip gap for various gap chord ratios.

Extracts from the high speed film record showing the blade motion in six configurations with smoke have been printed and are given in figs. 21-26.

5.2. Results

5.2.1. The static modes

The static deflection in flexure was found to be approximately proportional to the square of the distance from the root (fig. 9). It is clearly seen that the blade is stiffer when deflecting upwards than when deflecting downwards. This is due to the inability of the paper leading edge and the thread trailing edge to withstand compression. The torsional static mode was found to be approximately linear with the distance from the root (fig. 10).

The natural fundamental frequencies in torsion and

flexure as measured on the vibrating table were found to be approximately constant for all blades. It was also observed that a transverse vibration occurred at a frequency close to that of the natural fundamental frequency in torsion.

5.2.2. The effects of temperature, humidity and age of the blades

The flutter speed and frequency ratios obtained for any particular configuration showed no significant change with age with varying conditions of temperature and humidity, although there was a definite variation of the actual flutter speed and frequency. Even so, no correlation could be found between flutter speed, frequency, temperature and humidity, but the flutter speed was found to be reduced to approximately 0.9 of its value when the blade was new. This occurred after approximately 75 tests of about 2 to 3 minutes each, after which there was no appreciable change.

5.2.3. The flutter characteristics

5.2.3.1. Variation of the critical flutter speed ratio with gap chord ratio, stagger angle, inflow and camber (figs. 13 and 14)

It is seen that in general the critical flutter speed ratio, that is the ratio of the critical flutter speed of the aerofoil in cascade to the critical flutter speed of the isolated aerofoil, increases with increase of gap chord ratio and camber and decreases slightly with increase of stagger angle. Positive stagger angle is defined as leading edge down with respect to the axis of centres. The actual flutter speed was found to increase linearly with inflow over the range -5° to $+5^{\circ}$ whereas the flutter frequency ratio is approximately independent of inflow angle for a given gap chord ratio and stagger angle. (These effects are shown in fig. 11 for the isolated aerofoil case. Similar results were obtained for variable gap-chord ratio and stagger). Fig. 12 shows the increase of the modified speed ratio (V'_c/V_{co}) with inflow angle over a range of gap-chord ratios for zero stagger. Similar increases were obtained over the complete stagger angle range.

There are, however, several important variations from this general trend. At small stagger angles $-5^{\circ} \leq \beta \leq +5^{\circ}$ the flutter speed ratio increases monotonically with gap chord ratio and asymptotes to unity from below (see figs 13b and 13c). As the stagger angle becomes more negative the speed ratio exceeds unity for gap chord ratio $s/c \geq \frac{1}{2}$ and

then asymptotes to unity from above (see fig. 13a, 13b). For positive stagger angles $\beta > +5^{\circ}$ the flutter speed ratio increases up to $s/c = \frac{1}{2}$, has a minimum near $s/c = 3/4$ and thereafter increases monotonically (see fig. 13d, 13c). This effect is most marked at $\beta = +20^{\circ}$ (see fig. 13d) and appears to decrease in severity as the stagger is further increased (see fig. 13e).

Except for minor variations the effect of camber is to produce an overall increase in the values of the speed ratio which is least at the higher gap chord ratios.

It should also be noted that the variation from the general decrease of flutter speed ratio with increase of stagger (see fig. 14a,b,c) is most marked at $s/c = \frac{1}{2}$ and moderates with increase of gap chord ratio.

5.2.3.2. The variation of critical flutter frequency ratio and reduced frequency

(a) The critical flutter frequency ratio (Figs. 15 and 16)

For a cascade of symmetrical blades at zero stagger (see reference 2) the critical flutter frequency ratio decreases with gap chord ratio asymptoting to unity from above for large gap chord ratios. For the cambered blades it was found that the frequency ratio decreased sharply to a minimum at $s/c = \frac{1}{2}$ and approached unity as s/c became large (see figs. 15a,b,c,d,e). The actual minimum value of f'_{crit}/f_{crit} increased as the stagger angle was increased. The minimum was less marked at high positive stagger angles and appeared to occur at a slightly higher value of the gap chord ratio (see fig. 15e).

The critical flutter frequency ratio increased uniformly with stagger angle for all gap chord ratios (see figs. 16a,b,c), the increase being less marked at the higher values of gap chord ratio. The effect of camber was to reduce the frequency ratio by an approximately constant amount for a given gap chord ratio. For fixed gap chord ratio the difference between the curves for the 30° and 45° camber aerofoils decreased with increase of gap chord ratio.

(b) The reduced frequency ratio (Figs. 17 and 18)

The variation of the reduced frequency ratio with gap chord ratio was similar to the variation of the critical frequency ratio except that the position of the minimum was less marked at the positive stagger angles (see figs. 17c,d).

The variation of the reduced frequency ratio with stagger angle was similar to the variation of critical frequency ratio except that the curves showed a sharp increase in reduced frequency between -10° and 0° stagger angle (see figs. 18). The increase again moderated with increase in gap chord ratio and was negligible, within the accuracy of the experiment, for s/c greater than unity.

The curves of reduced frequency ratio show that for a given gap-chord ratio and stagger angle the difference between the reduced frequency ratios for the two cambers tested is greater than the corresponding difference in the critical frequency ratio. They also disclose a tendency for the reduced frequency ratios to diverge at the higher positive angles of stagger for a given gap chord ratio, and that the divergence increases with increase of gap chord ratio.

5.2.3.3. The aerofoil motion and the nature of flutter

From the study of the aerofoil motion under stroboscopic light, and from the high speed films it was noticed that there was a circular motion with frequency equal to approximately twice the flutter frequency superimposed upon the usual flexure-torsion motion, which was more pronounced in the 45° camber aerofoils than in the 30° camber aerofoils. It was also observed that, in the flexure-torsion motion, downward bending and nose-down torsion predominated. This may be seen in figs. 21-26.

A flexural oscillation of appreciable amplitude at a frequency varying between 1/3 and 1/2 of the measured flutter frequency was observed in many cases, especially at gap chord ratios less than 1 and at large positive or negative stagger angles. This oscillation commenced at a wind speed of about $0.9\ V'_{crit}$ and persisted after the flutter had stopped. It was also apparent with much smaller amplitude in other configurations.

At the lowest gap chord ratio (s/c = 1/4) the flutter starting and stopping speeds were well defined, but the amplitude was generally such that the trailing edges of adjacent blades frequency collided. It was therefore difficult to measure accurately the frequencies at speeds above the critical. At medium gap chord ratios (s/c less than 1) a pulsating flutter was observed at all stagger angles. This consisted mainly of a cyclic amplitude variation of low but erratic frequency, the actual flutter frequency being unaffected within the accuracy of the measurements.

In several cases flutter was not initiated naturally

but adjacent aerofoils merely diverged until the tips touched. They remained in that position, and flutter could not then be started by either manual excitation of the aerofoils or by disturbing the freestream ahead of the aerofoils. This divergence effect seemed to be random in occurrence and confined to gap chord ratios less than 1, and small angles of stagger.

5.2.3.4. The effect of tip clearance (fig. 19)

As the tip clearance was reduced the ratio of the critical flutter speed of the cascade with finite tip gap to the critical flutter speed of the cascade with infinite tip gap was reduced. It was found that increase in gap chord ratio gave a decrease of this speed ratio. For gap chord ratios greater than 3/4 no significant difference, at a given tip clearance, was observed. It was shown that stagger angle had no effect on this ratio.

6. Discussion

6.1. The accuracy of the results

Although the models had not exactly similar properties and the speed and frequency measurements were only accurate to about 1 per cent it is believed that, due to the large number of tests and the consistency between them, the mean values of the ratios as presented in the figures give a reliable representation of the characteristics of the flexure-torsion flutter of cambered aerofoils in cascade, particularly as the effects of ageing and of variations of temperature and humidity were eliminated as far as possible. The non-dimensional presentation of the results should make them of general application unless the extreme flexibility of the aerofoils allows motions which do not occur with the stiffer models. This will be discussed more fully later.

6.2. The flutter characteristics

As the gap-chord ratio and the stagger angle are altered the behaviour of the critical flutter speed and frequency ratios for the cambered blades shown features which are absent in the results for symmetrical blades (ref. 2). Under stroboscopic light and from the examination of the high speed film records it was seen that boundary layer separation occurred on the upper surface of the cambered aerofoil very soon after the downgoing motion commenced. Separation also occurred close to the leading

edge on the under surface at the position of maximum negative twist. This is shown particularly in figs.22-24. (A similar upper surface effect has been observed on a symmetrical aerofoil oscillating in a smoke tunnel). Due to the surface roughness of the models it is probable that transition occurred very close to the leading edge. Thus the boundary layer separation on the upper surface was turbulent and not a laminar separation.

At negative stagger angles the separation effect is reduced, separation appearing to start further aft on the upper surfaces particularly at the lower gap-chord ratios and higher angles of stagger. For positive stagger angles the separation appears to occur further forward on the upper surfaces, again particularly at the lower gap-chord ratios and higher stagger angles. With negative stagger the aft movement of the separation position on the upper surface of a given aerofoil is probably due to the suction on the rear part of the upper surface of the adjacent aerofoil below. The forward movement of separation with positive stagger is likewise probably due to the effect of the suction on the forward part of the aerofoil next above and the subsequent sudden deceleration in the passage between the blades. The marked changes in the curves of critical flutter speed ratio and reduced frequency ratio (figs. 14 and 16) in the range of small stagger angle may indeed be due to this rapid change of separation position. It should be noted that this effect is more marked with larger camber.

It is suggested that the boundary layer separation effects will give rise to changes in the aerodynamic derivatives* of a cascade of cambered blades in addition to those mentioned in reference 2 for symmetrical aerofoils. Further it is believed that the significance of these changes will be realised, and the behaviour of the critical speed and frequency ratios explained, only when the magnitude and relative importance of the various derivatives have been determined from a theoretical investigation.

---

* Changes in the aerodynamic derivatives with change in transition position on oscillating rigid symmetrical aerofoils in cascade have been found by Milne and Willox, (College of Aeronautics Report No. 93).

6.3. The aerofoil motion and nature of flow

From examinations under stroboscopic light and of the slower speed films taken when the aerofoils were comparatively new it was seen that adjacent aerofoils moved in anti-phase except for slight variations at the large angles of stagger. Figures 21-26 do not show a motion of this nature but it should be remembered that the aerofoils were considerably aged and had widely differing mechanical properties when these films were taken.

The circular motion superimposed on the normal flexure torsion motion is most likely due to drag changes coupled with changes in lift and to a lesser extent the natural transverse vibration of the aerofoil mentioned in section 5.2.1. It can be shown theoretically that an aerofoil fluttering will experience a thrust force of period equal to twice the flutter frequency. In some cases this motion caused a premature failure of the paper-reinforced leading edge near the root.

The flexural in-phase oscillation observed before the commencement of flutter has also been noted by Kilpatrick and Ritchie (ref. 8) when performing stress determination tests on metal compressor blades. It is suggested that this may be due to excitation being fed upstream from the turbulent wake.

The pulsating flutter consists of an amplitude variation of uncertain frequency in the torsional mode and does not appear in the flexural mode. This may be caused by some instability in the flow the exact nature of which is not known.

The divergence of the aerofoils noted in section 5.2.3.3. was random in occurrence and so far no satisfactory explanation has been found to account for it.

6.4. The modes of vibration

In the determination of the static modes it was noted that there was some difference between the up and the down deflection mode and between the positive and negative twisting modes. These differences are not sufficient to account for the absence of up flexure and the very small nose up twisting as noted in section 5.2.3.3 (figs. 21-26).

It is felt that a knowledge of the dynamic modes during flutter is essential if flutter calculations are to be made. The measurement of the dynamic modes is inherently difficult but high speed photography with sharp definition should provide a means of obtaining these modes with sufficient accuracy.

6.5. Tip clearance

The reduction in the modified flutter speed ratio of fig. 19 with reduction of tip clearance is explained immediately by consideration of the image of the tip vortex in the perspex wall. With decrease in gap chord ratio the interference between the tips of adjacent blades reduces the strength of the tip vortex and hence of the image system. This accounts for the lessening of the tip effect for small gap chord ratios.

These results are only to be regarded as an indication of this effect and it is suggested that further detailed experiments be performed particularly with smaller and more accurately maintained tip clearances.

6.6. Application of the results and suggestion for further study

It should be appreciated that these results could only be applied generally to aerofoils having distributed mass and stiffnesses if such aerofoils oscillated in a manner similar to that of the aerofoils under discussion.

It is suggested that further study be uhdertaken to investigate the effect of cascading on the aerodynamic flutter derivatives and to obtain more detailed information concerning the nature of the flow over the fluttering aerofoils.

7. Conclusions

1. The effect of camber is to increase the critical flutter speed ratio and decrease the critical frequency ratio for any given value of gap chord ratio.

2. Stagger has an appreciable effect on the flutter characteristics of a cascade of cambered aerofoils. Negative stagger angles further increase the critical flutter speed ratio and decrease the critical frequency ratio so that the critical flutter speed of a cascade of cambered aerofoils can be greater than the critical flutter speed of an isolated aerofoil, and the critical flutter frequency can be much lower. Positive stagger angles decrease the flutter speed ratio and increase the flutter frequency ratio.

3. For gap chord ratios greater than 1/4 and stagger angles less than $+20^{\circ}$ the flutter frequency ratio is less than unity, in distinction to the results for symmetrical aerofoils.

4. Incidence in the range $-2^{\circ} \leq a \leq 2^{\circ}$ has little influence on the flutter speed and frequency ratios.

5. The phase difference between the motion of two adjacent aerofoils is very nearly 180°.

6. The critical flutter speed ratio is reduced considerably with reduction in tip clearance. The effect is aggravated with increase of gap chord ratio. Tip clearance has little effect on the critical flutter frequency ratio.

8. Acknowledgements

The authors wish to express their gratitude to the Director of the Royal Aircraft Establishment for the serivces rendered in connection with the high-speed photographs.

The guidance and helpful discussions given by Professor J.A.J. Bennett and Mr. G.M. Lilley are gratefully acknowledged and the authors' thanks are extended to Mr. S.H. Lilley, Mr. C.D. Bruce and Mr. L. Wilsher for their assistance in the preparation of the apparatus.

9. References

1. Ch. Bellenot and J. Lalive d'Epinay — Self induced vibrations of turbo-machine blades. Brown Boveri Review, Vol. 37, pp.368-376, 1950.

2. G.M. Lilley — An investigation of the flexure-torsion flutter characteristics of aerofoils in cascade. College of Aeronautics Report No. 60, 1952.

3. M.A. Sheikh — An investigation of the flexure-torsion flutter characteristics of aerofoils in cascade. College of Aeronautics, unpublished note, 1953.

4. A. Mendelson and R.W. Carroll — Lift and moment equations for oscillating airfoils in an infinite unstaggered cascade. N.A.C.A. T.N. 3263, 1954.

5. F. Sisto — Unsteady aerodynamic reactions on airfoils in cascade. Jnl. of Aero. Sciences, May 1955, pp.297-302.

6. R. Legendre — Premiers elements d'un calcul de l'amortissement aerodynamique des vibrations d'aubes de compresseurs. La Recherche Aeronautique No. 37, Jan.-Feb. 1954.

7. E.A. Eichelbrenner — Application numerique d'un calcul d'amortissement aerodynamique des vibrations d'aubes de compresseurs. La Recherche Aeronautique No. 46, July-Aug. 1955.

8. D.A. Kilpatrick and J. Ritchie — Compressor cascade flutter tests. N.G.T.E. Reports Nos. 133 and 163.

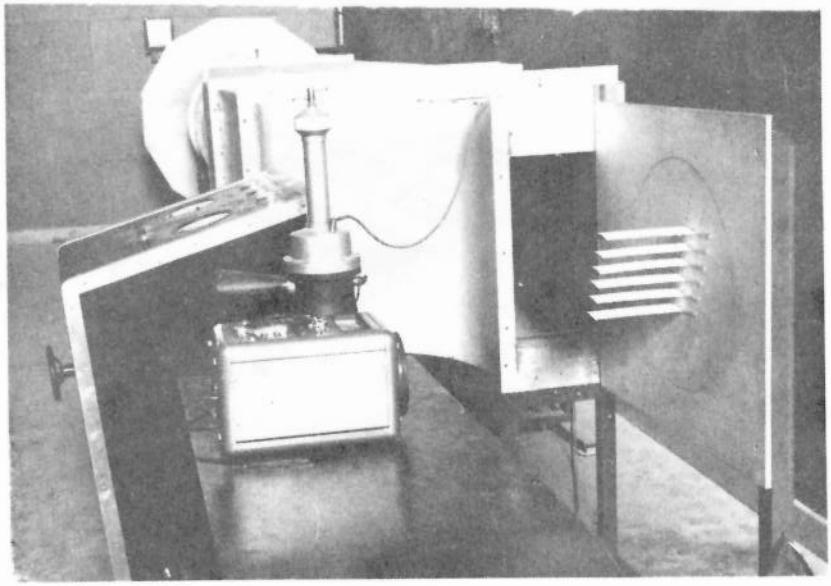

GENERAL ARRANGEMENT OF TUNNEL
AND THE MODELS.

FIG.1

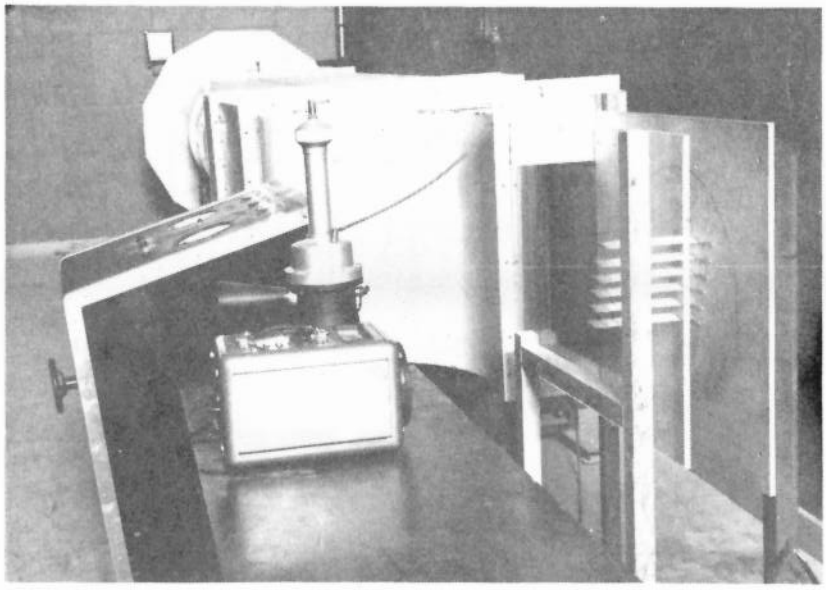

THE PERSPEX PLATE IN POSITION
FOR TIP GAP TESTS
FIG.2

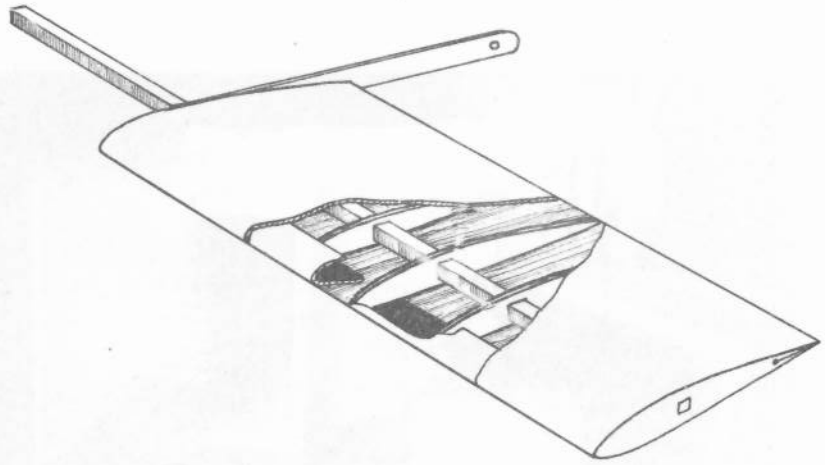

PART SECTIONAL VIEW OF A TYPICAL
FIG. 3 MEMBER OF THE CASCADE.

WING SECTION: NACA 0010 ON CIRCULAR ARC CAMBER LINES OF 45° & 30°.

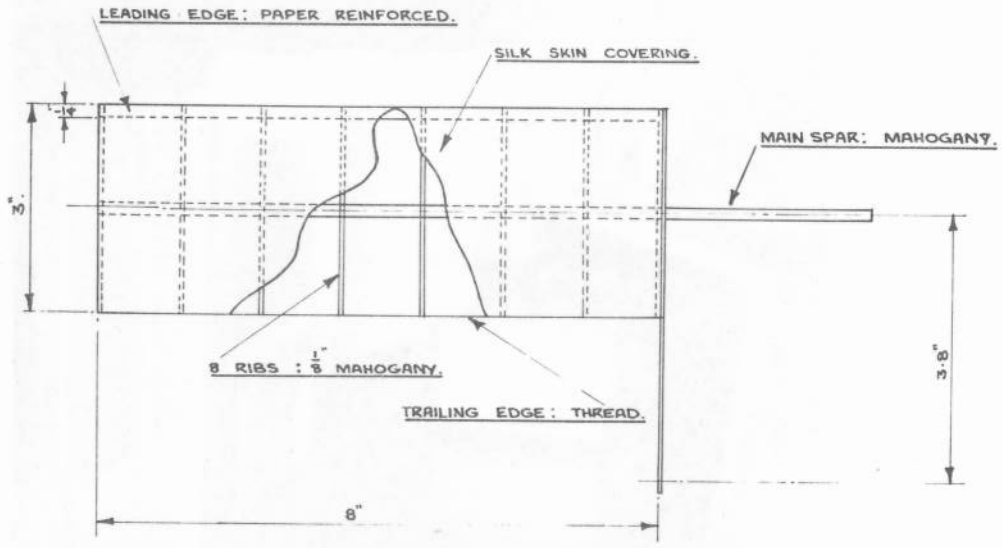

GENERAL DETAILS OF A TYPICAL
FIG. 4 MEMBER OF THE CASCADE.

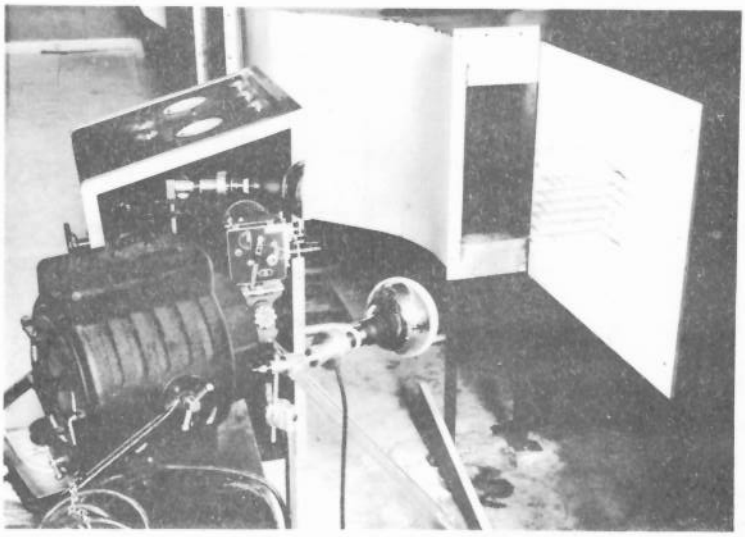

FIG. 5 ARRANGEMENT OF THE PHOTOGRAPHIC EQUIPMENT.

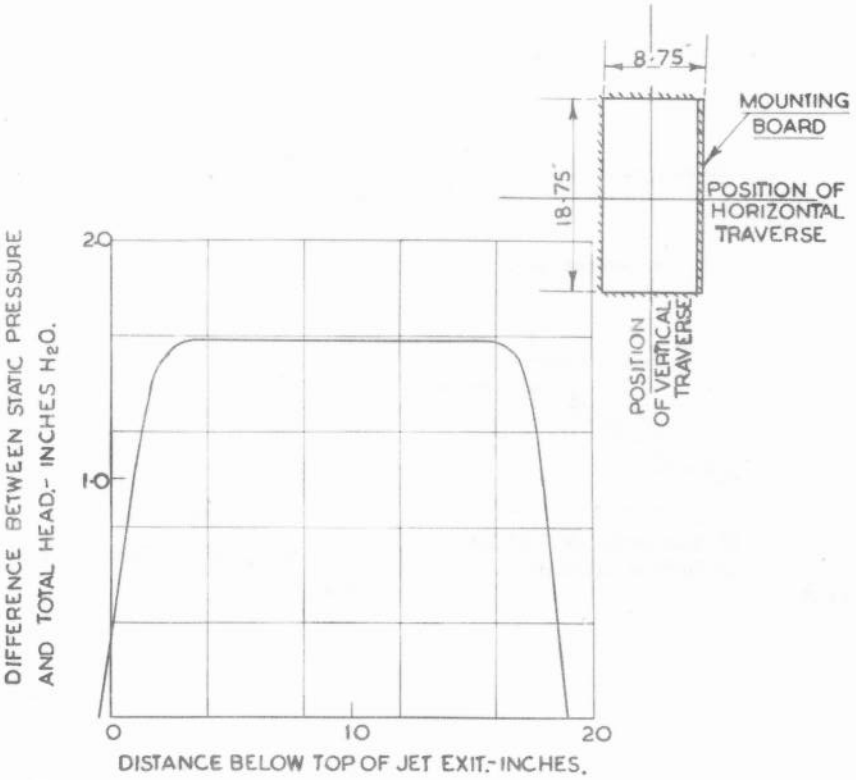

FIG. 6 VERTICAL TOTAL HEAD TRAVERSE AT BLADE ATTACHMENT POSITION 18 INS. DOWNSTREAM OF NOZZLE. WIND SPEED 82·5 FEET PER SECOND.

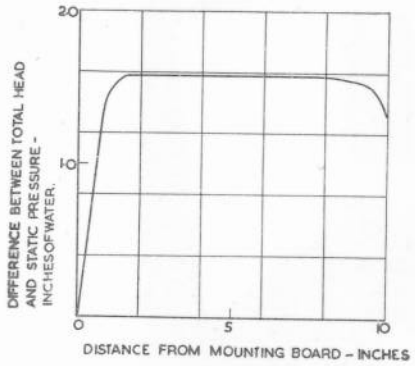

HORIZONTAL TOTAL HEAD TRAVERSE AT BLADE ATTACHMENT POSITION 18INS. DOWNSTREAM OF NOZZLE. WIND SPEED 82·5 FT/SEC.

FIG.7

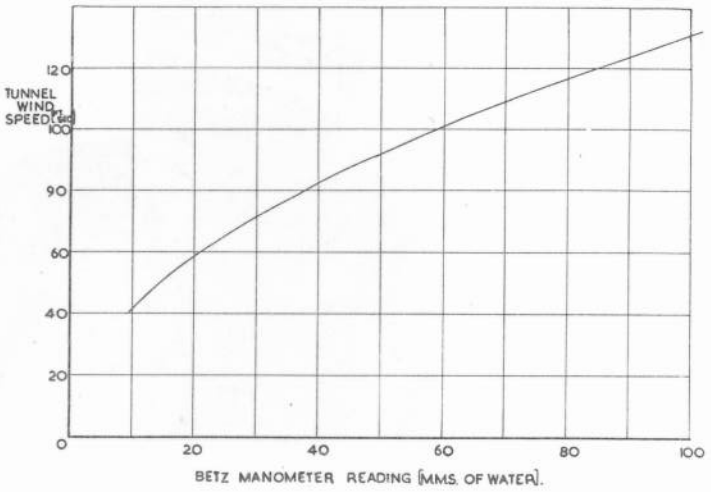

TUNNEL SPEED CALIBRATION CURVE.

FIG.8

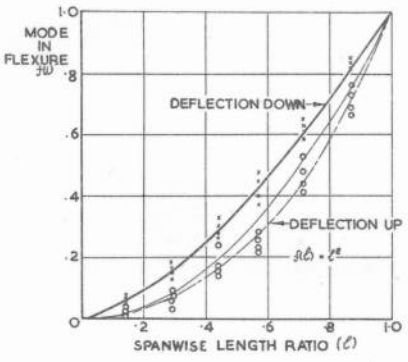

DEFLECTION MODE IN FLEXURE FOR TYPICAL AEROFOIL

FIG.9

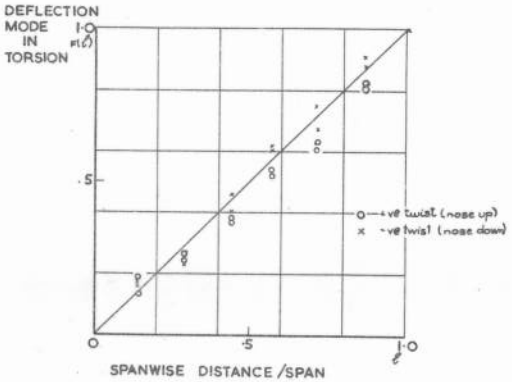

TYPICAL DEFLECTION MODE IN TORSION

FIG.10

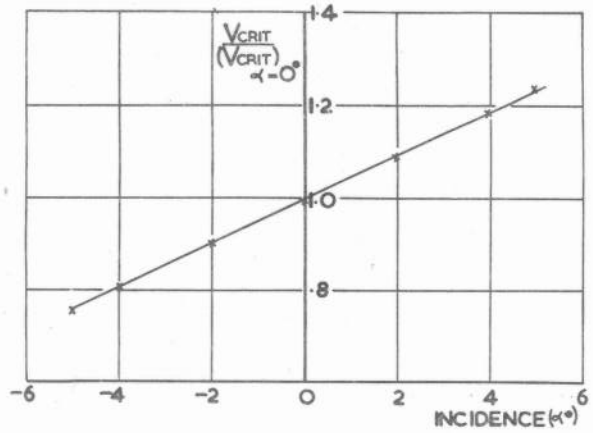

VARIATION OF CRITICAL FLUTTER SPEED WITH INCIDENCE

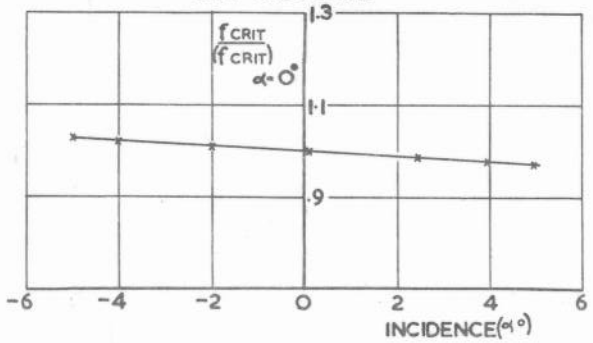

VARIATION OF CRITICAL FLUTTER FREQUENCY WITH INCIDENCE

FIG. 11 THE FLUTTER CHARACTERISTICS OF THE ISOLATED AEROFOIL CAMBER 30°

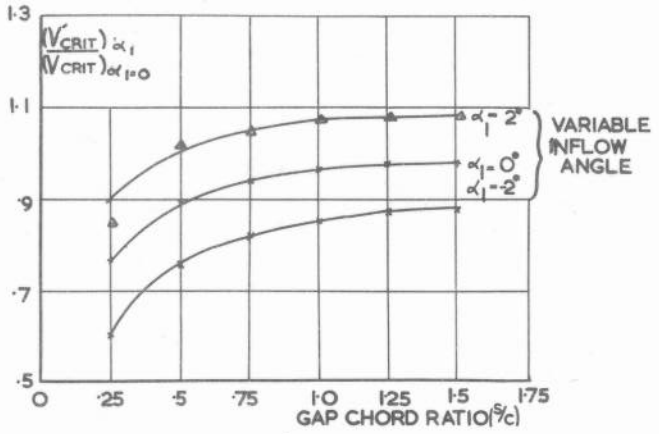

VARIATION OF $\frac{\text{CRITICAL FLUTTER SPEED FOR CASCADE } (V_{CRIT})\,\alpha_1}{\text{CRITICAL FLUTTER SPEED FOR ISOLATED AEROFOIL AT ZERO INFLOW ANGLE } (V_{CRIT})\,\alpha_1=0°}$ WITH GAP-CHORD RATIO

FIG. 12.

CAMBER 30°
STAGGER 0°

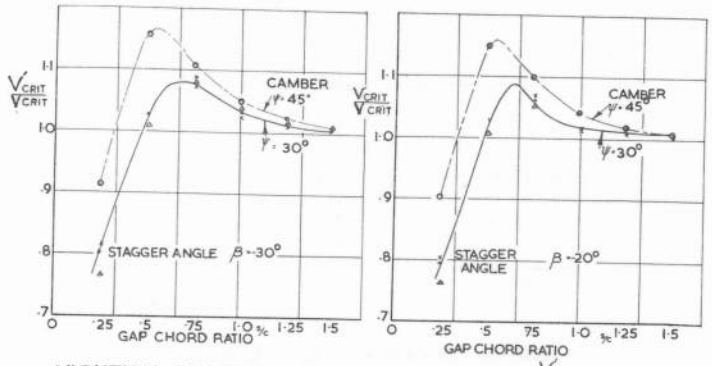

VARIATION OF CRITICAL FLUTTER SPEED RATIO $\frac{V_{CRIT}}{V_{CRIT}}$ WITH GAP CHORD RATIO s/c

FIG.13A.

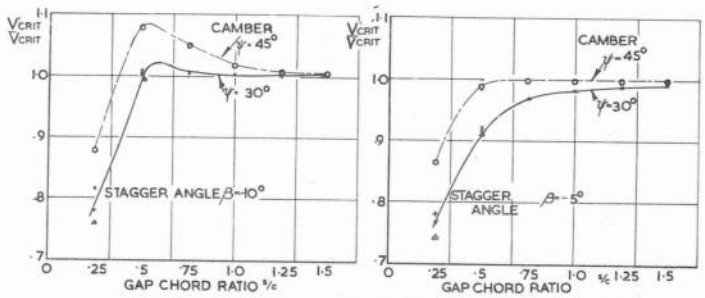

VARIATION OF CRITICAL FLUTTER SPEED RATIO $\frac{V_{CRIT}}{V_{CRIT}}$ WITH GAP CHORD RATIO. s/c

FIG.13B

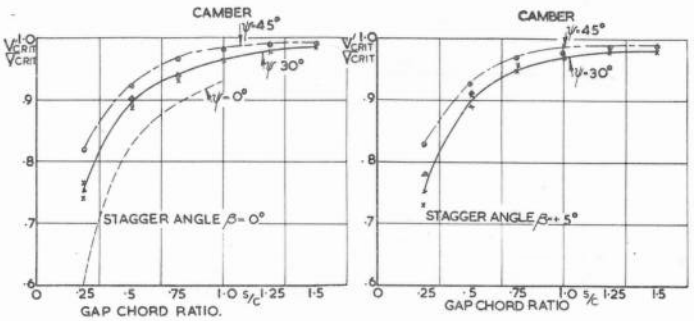

VARIATION OF CRITICAL FLUTTER SPEED RATIO $\frac{V_{CRIT}}{V_{CRIT}}$ WITH GAP CHORD RATIO. s/c

FIG.13C

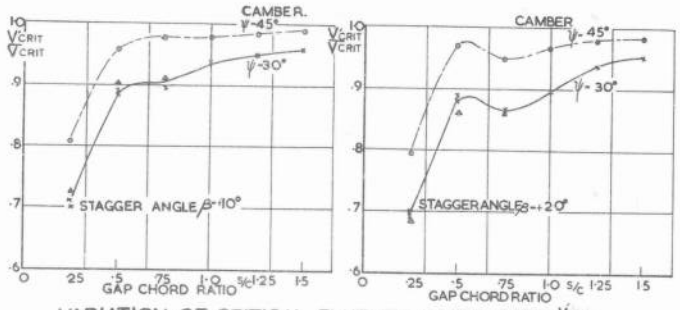

VARIATION OF CRITICAL FLUTTER SPEED RATIO $\frac{V_{CRIT}}{V_{CRIT}}$
FIG 13 D. WITH GAP CHORD RATIO S/C.

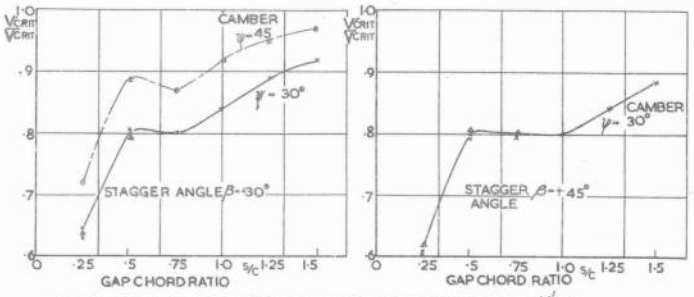

VARIATION OF CRITICAL FLUTTER SPEED RATIO $\frac{V_{CRIT}}{V_{CRIT}}$
FIG 13E WITH GAP CHORD RATIO S/C

LEGEND

+ 30° CAMBER ZERO INCIDENCE
X 30° CAMBER −2° INCIDENCE
△ 30° CAMBER +2° INCIDENCE
○ 45° CAMBER ZERO INCIDENCE

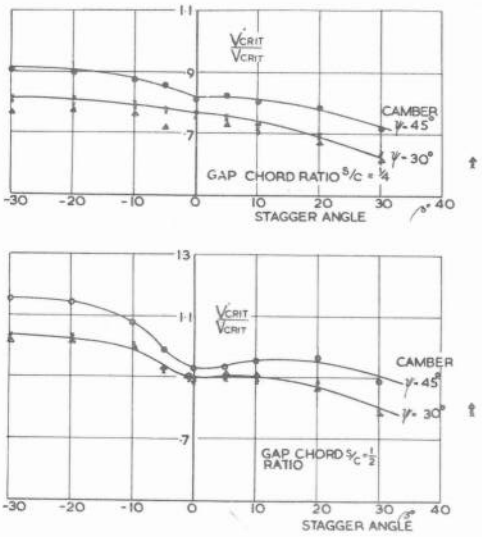

VARIATION OF CRITICAL FLUTTER SPEED RATIO $\left(\frac{V_{CRIT}}{V_{CRIT}}\right)$ WITH STAGGER ANGLE β

FIG.14A

LEGEND

+ 30° CAMBER ZERO INCIDENCE

X 30° CAMBER -2° INCIDENCE

Δ 30° CAMBER +2° INCIDENCE

⊙ 45° CAMBER ZERO INCIDENCE

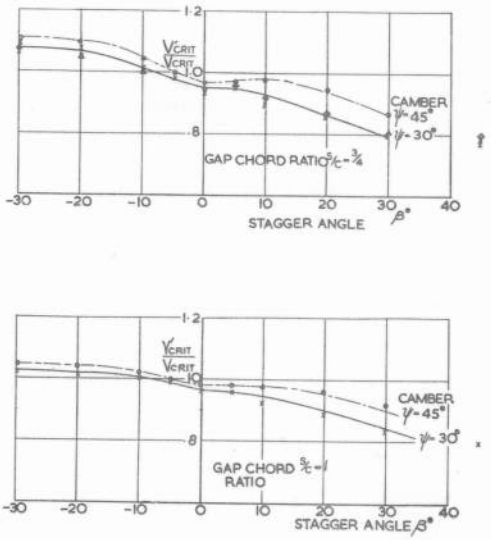

VARIATION OF CRITICAL FLUTTER SPEED RATIO $\frac{V_{CRIT}}{V_{CRIT}}$ WITH STAGGER ANGLE β

FIG.14B

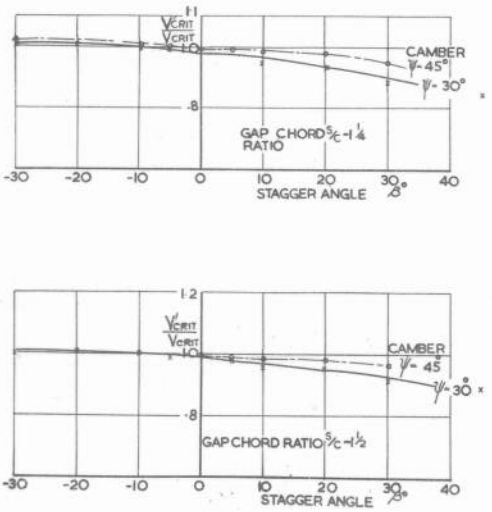

VARIATION OF CRITICAL FLUTTER SPEED RATIO $\frac{V_{CRIT}}{V_{CRIT}}$ WITH STAGGER ANGLE β

FIG.14C.

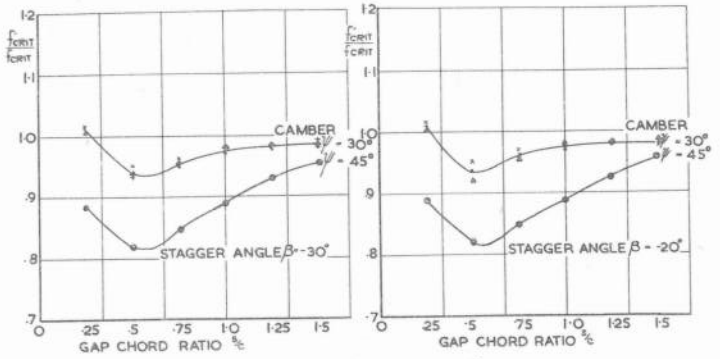

FIG 15A VARIATION OF CRITICAL FREQUENCY RATIO $\frac{f_{CRIT}}{f_{CRIT}}$ WITH GAP CHORD RATIO $\frac{s}{c}$

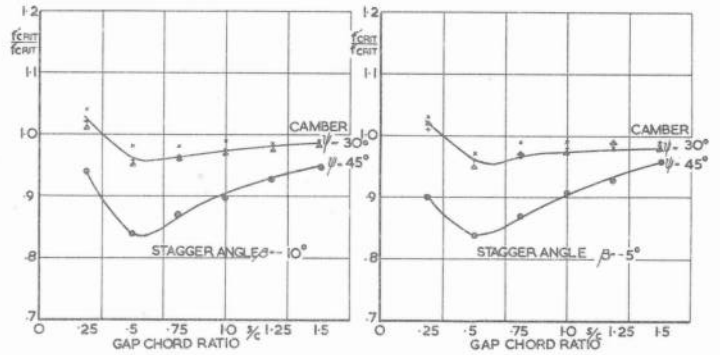

FIG 15B. VARIATION OF CRITICAL FREQUENCY RATIO $\frac{f_{CRIT}}{f_{CRIT}}$ WITH GAP CHORD RATIO $\frac{s}{c}$

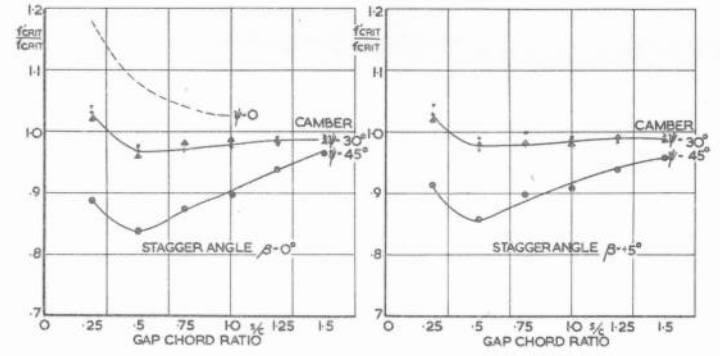

FIG. 15C VARIATION OF CRITICAL FREQUENCY RATIO $\frac{f_{CRIT}}{f_{CRIT}}$ WITH GAP CHORD RATIO $\frac{s}{c}$

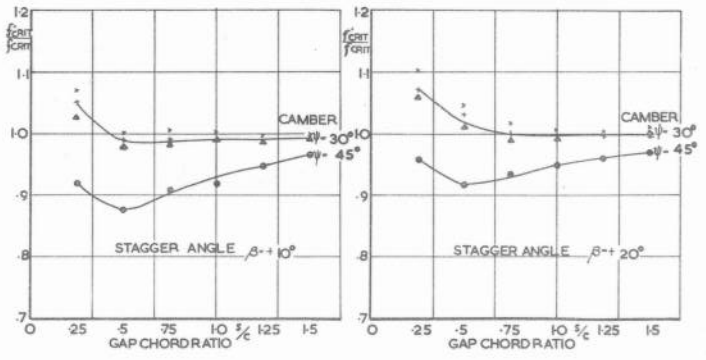

FIG.15D VARIATION OF CRITICAL FREQUENCY RATIO $\frac{f_{CRIT}}{f_{CRIT}}$ WITH GAP CHORD RATIO $\frac{s}{c}$

LEGEND

+ 30° CAMBER ZERO INCIDENCE
X 30° CAMBER -2° INCIDENCE
Δ 30° CAMBER +2° INCIDENCE
⊙ 45° CAMBER ZERO INCIDENCE

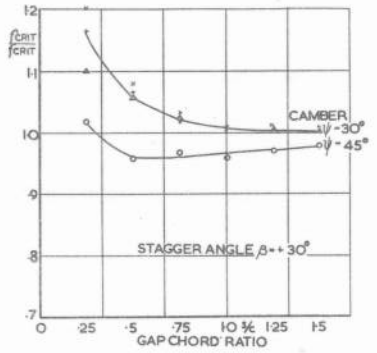

FIG.15E VARIATION OF CRITICAL FREQUENCY RATIO $\frac{f_{CRIT}}{f_{CRIT}}$ WITH GAP CHORD RATIO $\frac{s}{c}$

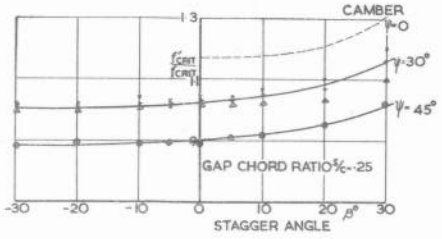

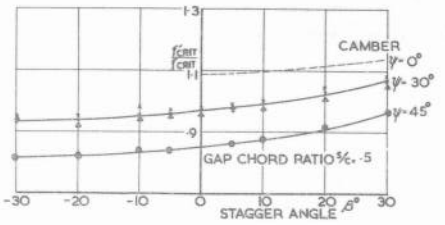

VARIATION OF CRITICAL FREQUENCY RATIO $\frac{f_{CRIT}}{f_{CRIT}}$ WITH STAGGER ANGLE β

FIG.16A

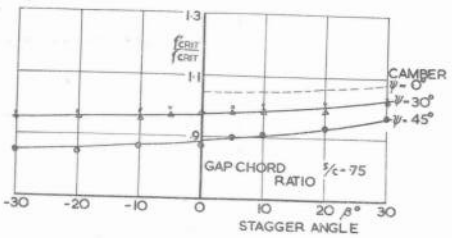

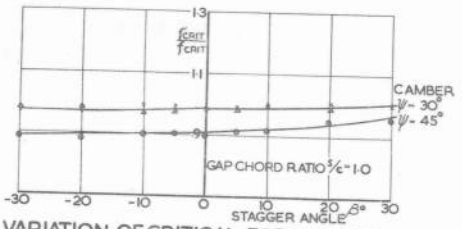

VARIATION OF CRITICAL FREQUENCY RATIO $\frac{f_{CRIT}}{f_{CRIT}}$ WITH STAGGER ANGLE β

FIG.16B

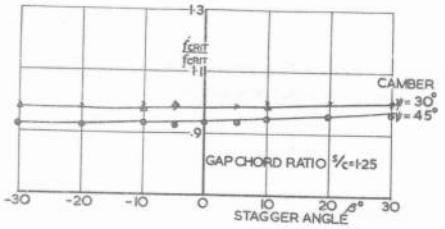

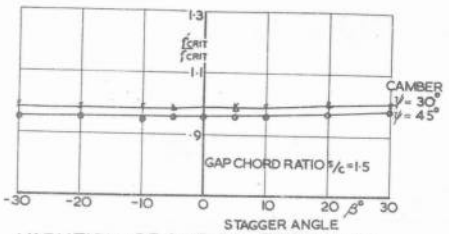

LEGEND
+ 30° CAMBER ZERO INCIDENCE
X 30° CAMBER −2° INCIDENCE
Δ 30° CAMBER +2° INCIDENCE
⊙ 45° CAMBER ZERO INCIDENCE

VARIATION OF CRITICAL FREQUENCY RATIO $\frac{f_{CRIT}}{f_{CRIT}}$ WITH STAGGER ANGLE β

FIG.16C

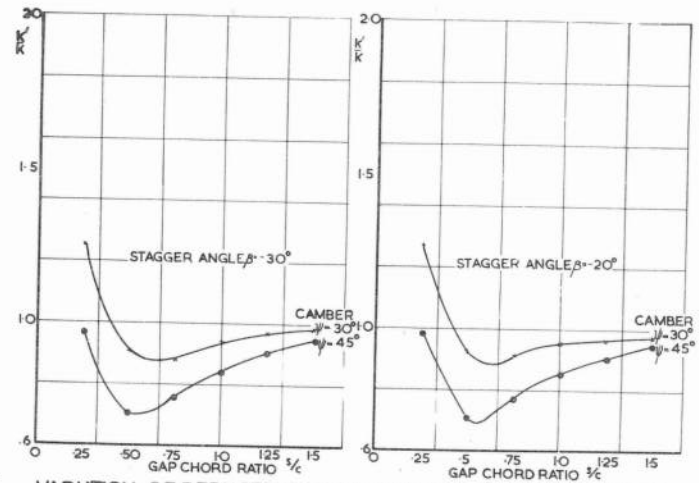

FIG.17A VARIATION OF REDUCED FREQUENCY RATIO(K'_k) WITH GAP-CHORD RATIO(S/c)

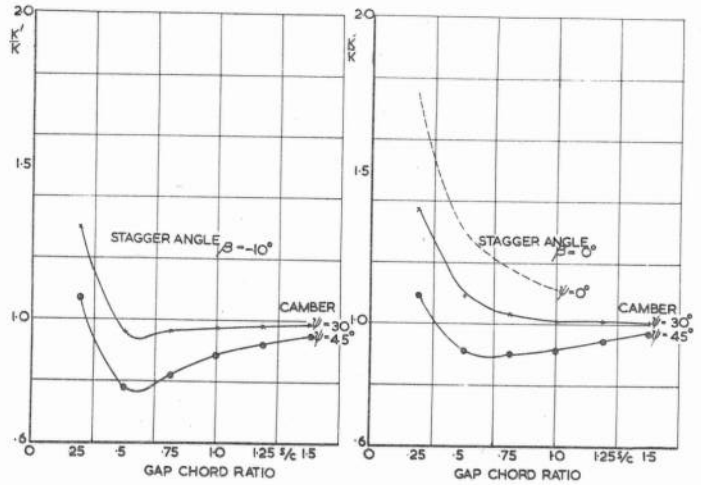

FIG.17B VARIATION OF REDUCED FREQUENCY RATIO(K'_k) WITH GAP CHORD RATIO(S/c).

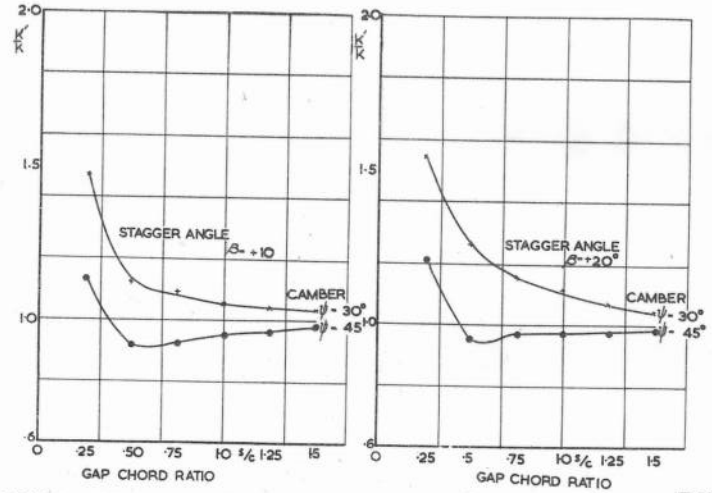

FIG.17C VARIATION OF REDUCED FREQUENCY RATIO(K'_k) WITH GAP-CHORD RATIO(S/c).

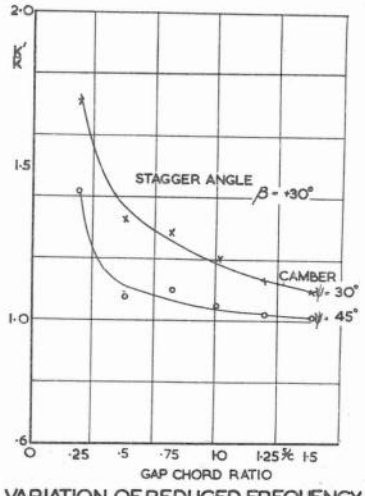

FIG.17D VARIATION OF REDUCED FREQUENCY RATIO(K'_k) WITH GAP-CHORD RATIO(S/c)

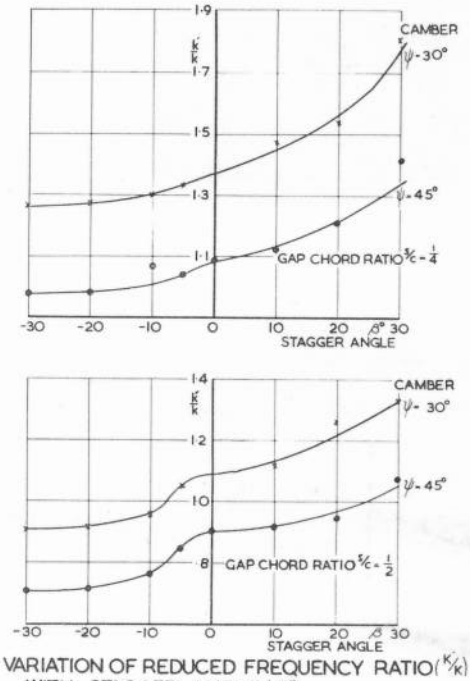

VARIATION OF REDUCED FREQUENCY RATIO (K'/k) WITH STAGGER ANGLE (β)

FIG.18A

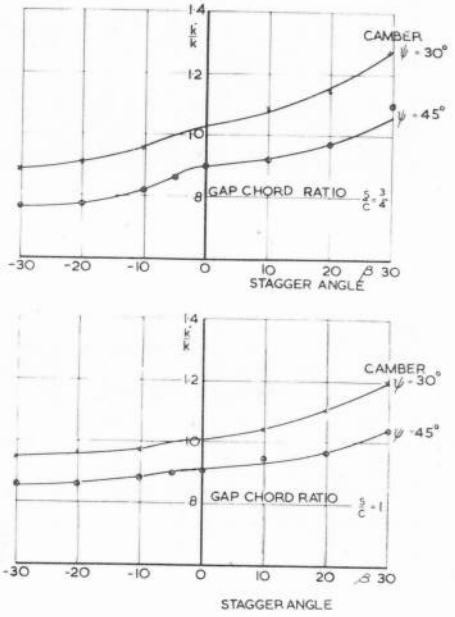

VARIATION OF REDUCED FREQUENCY RATIO (K/k) WITH STAGGER ANGLE ($\beta°$)

FIG.18 B.

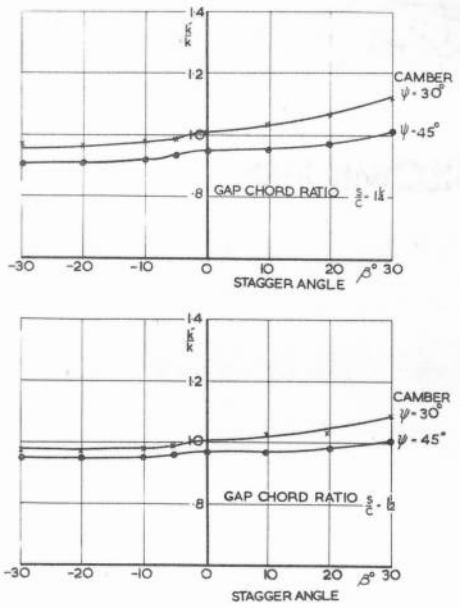

VARIATION OF REDUCED FREQUENCY RATIO WITH STAGGER ANGLE ($\beta°$)

FIG.18C.

LEGEND

× 30° CAMBER ZERO INCIDENCE

⊗ 45° CAMBER ZERO INCIDENCE

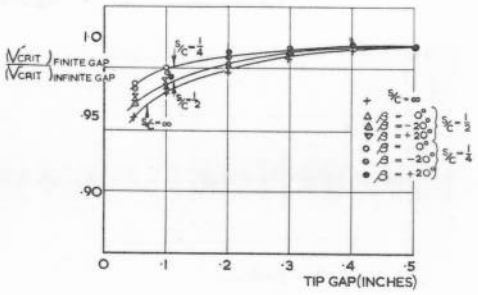

VARIATION OF CRITICAL FLUTTER SPEED RATIO $\frac{(V_{CRIT})_{FINITE\ GAP}}{(V_{CRIT})_{INFINITE\ GAP}}$ WITH TIP GAP FOR VARIOUS GAP CHORD RATIOS (s/c)

FIG. 19

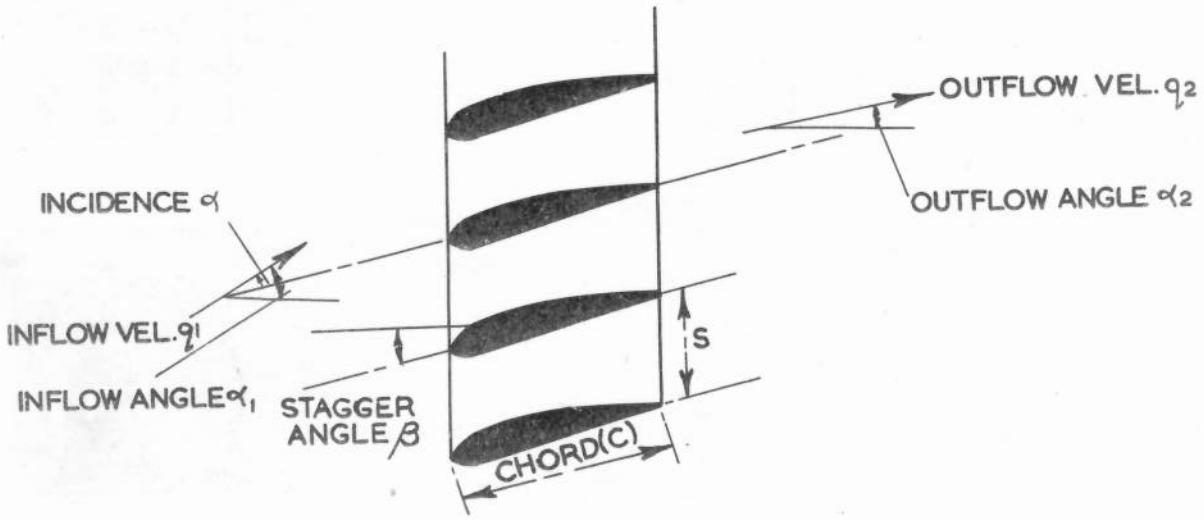

FIG.20. CASCADE GEOMETRY

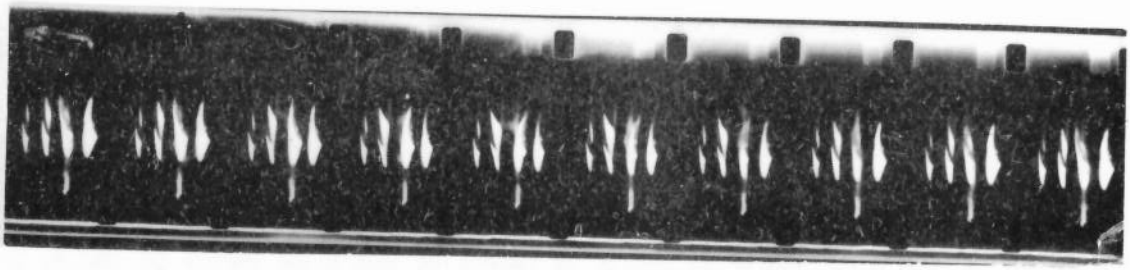

FIG. 21

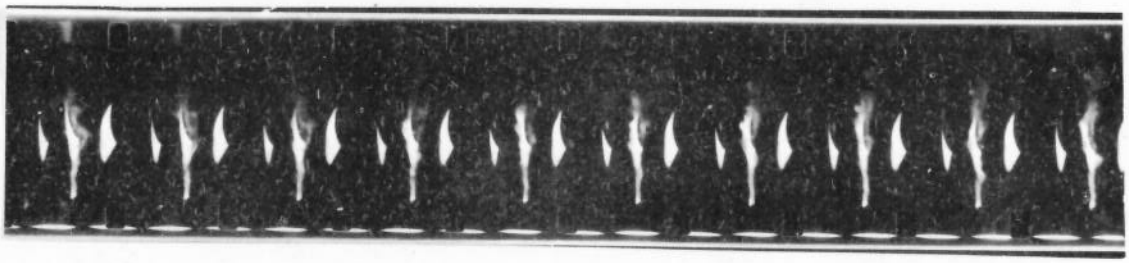

FIG.22

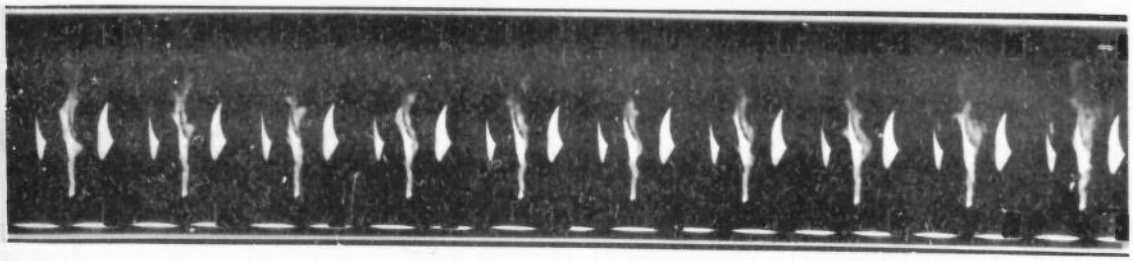

FIG.22A

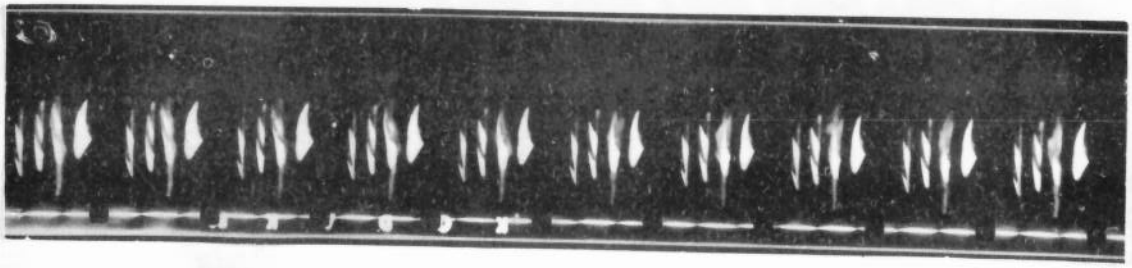

FIG. 23

HIGH SPEED CINÉ FLOW VISUALISATION RECORDS OF THE CASCADE IN FLUTTER USING A SINGLE SMOKE FILAMENT.

FIG. 21-23

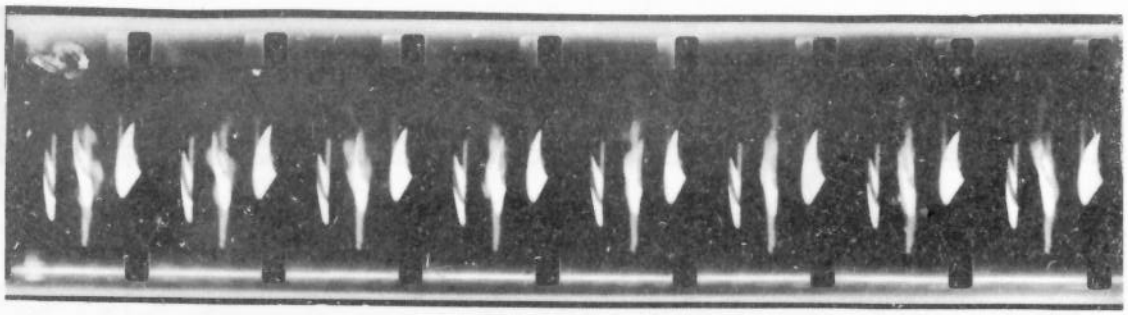

FIG.24

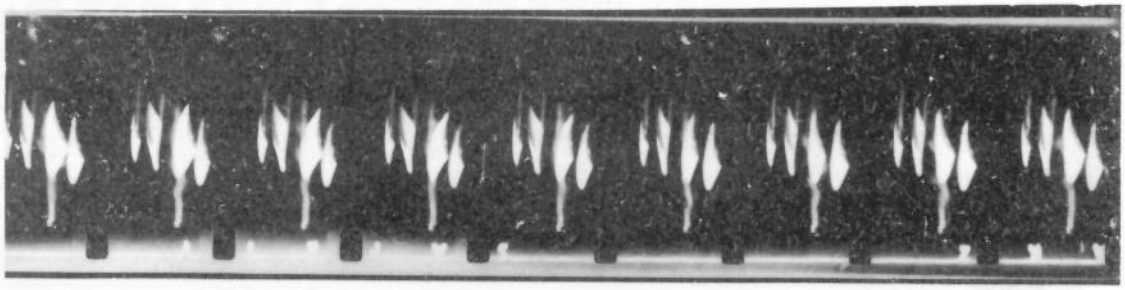

FIG.25

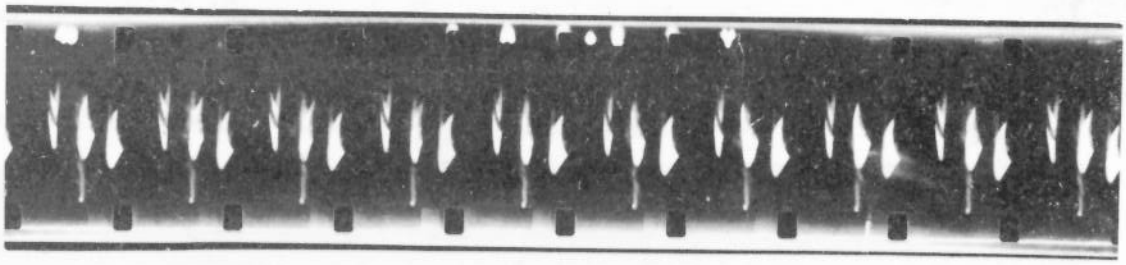

FIG.26

FIGURE	STAGGER ANGLE DEGREES	GAP CHORD RATIO	FILM SPEED FRAMES/SEC.	AIR SPEED FT./SEC.	FLUTTER FREQUENCY C.P.S.
21	0	1/2	400	60	40
22.22A	0	3/4	650	65	34
23	-20	1/2	600	65	33
24	-20	3/4	250	70	33
25	+20	1/2	350	60	36
26	+20	3/4	400	60	36

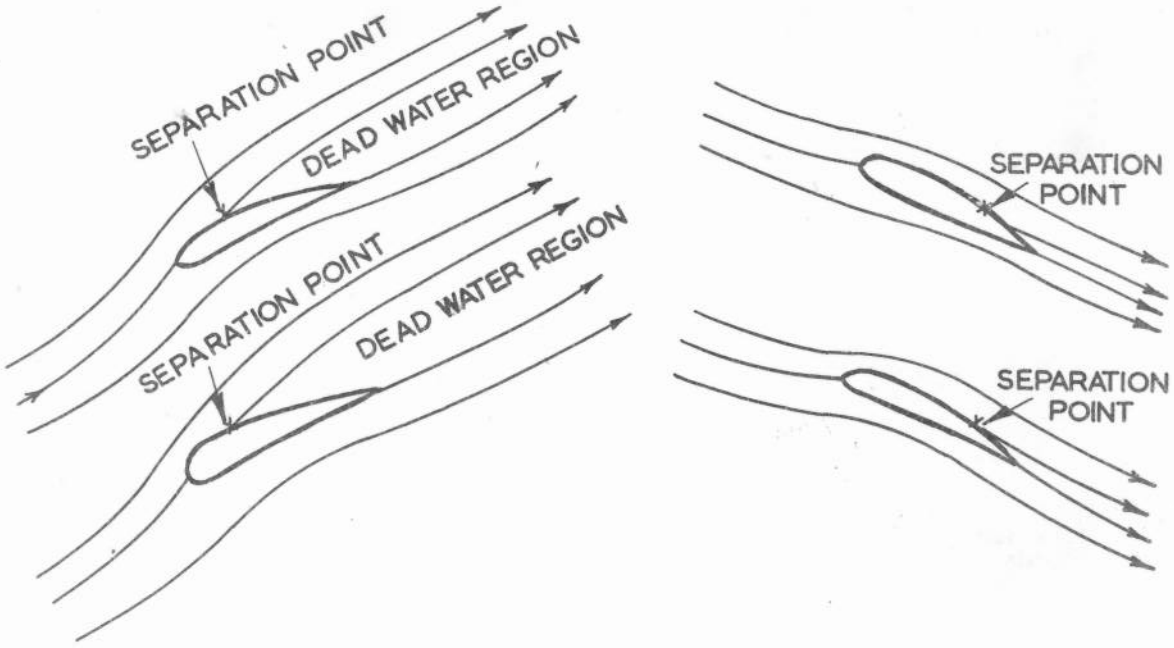

$\beta > 0$ $\beta < 0$

FIG.27. THE MOVEMENT OF THE SEPARATION POINT WITH CHANGE OF STAGGER ANGLE